Bulletin of the Seismological Society of America, Vol. 96, No. 3, pp. 879–897, June 2006, doi: 10.1785/0120050138

A New Attenuation Relation for Strong Ground Motion in Japan Based on Recorded Data

by Tatsuo Kanno, Akira Narita, Nobuyuki Morikawa, Hiroyuki Fujiwara, and Yoshimitsu Fukushima

Abstract Following the 1995 Hyogo-ken Nanbu Kobe. Earthquake, the Japanese government, in an effort to prevent future earthquake disasters, installed networks consisting of a large number of strong-motion observation stations. Further, national seismic hazard maps were made available to the public on an Internet website in March 2005 by the Headquarters for Earthquake Research Promotion. However, these maps indicate only the local seismic intensity for Japan, as empirically converted from predicted peak velocity in consolidated soils. For various applications, other strong-motion indexes such as the response spectral acceleration are required. In this study, a database of whole Japanese strong ground motion records between 1963 and 2003 is established in order to identify a new standard attenuation relation for Japan, for response acceleration as well as peak value. It is usually very difficult to determine a suitable model form due to the large variability of strong-motion data and correlation among the model variables, because the strong coupling of variables in an attenuation model, and the statistical power of the data is often not large enough to determine the necessity of these parameters. Therefore, in this study, our model has only three variables: earthquake magnitude, shortest distance to the seismic fault plane, and focal depth. To improve predictions given by the model, site correction terms are adopted and additional terms for correcting regional anomalous seismic intensity with respect to the base model are determined. The good fit between the model and observed strong-motion records suggests that the new model is reasonably robust.

Introduction

Following the 1995 Hyogo-ken Nanbu, Kobe earthquake, the Japanese government, in an effort to prevent future earthquake disasters, installed networks consisting of a large number of strong-motion observation stations, including K-NET (Kinoshita, 1998), which is operated by the National Research Institute for Earth Science and Disaster Prevention. Further, national seismic hazard maps were made public on an Internet website in March 2005 by the Headquarters for Earthquake Research Promotion (1995).

These maps indicate only the local seismic intensity for Japan, as empirically converted from peak velocity predicted by Si and Midorikawa (1999) in consolidated soils. For various applications, other strong-motion indexes such as the response spectral acceleration are required. Some empirical attenuation relations for the response spectra (e.g., Kobayashi and Midorikawa, 1982; Annaka *et al.*, 1997) exist for Japan, but they were derived from a limited set of records. In this study, a database of whole Japanese strong ground motion records between 1963 and 2003 is established in order to identify a new standard attenuation relation for Japan, for response acceleration as well as peak ground acceleration (PGA) and velocity (PGV).

It is usually very difficult to determine a suitable model form due to the large variability of strong-motion data and correlation among the model variables, because the strong coupling of variables in an attenuation model and the statistical power of the data is often not large enough to determine the necessity of these parameters (Fukushima and Tanaka, 1990). Therefore, we attempt to determine a simple form for average characteristics only with minimum parameters. The effects of other confusing parameters such as site geology, regional anomalies, and so forth will be corrected by bias reduction of residuals. This kind of correction has succeeded in the past; for example, the Nishimura and Horike (2003) model has additional parameters to accommodate those records that have large and systematic residuals, and Morikawa *et al.* (2003) determined additional correction terms for the Si and Midorikawa (1999) model to better predict the anomalous seismic intensity area in northeast Japan.

Since confusing near-source phenomena can be ex-

pected, theoretical approaches are valuable for very short fault-to-site distances. Nevertheless, ground motions simulated by theoretical methods are strongly dependent on the assumed model and not always warranted by the observations. These simulated results should be compared with average values estimated by an empirical attenuation relation. As a matter of course, a standard attenuation relation is very useful for probabilistic seismic hazard analysis and will be essential to a future national seismic hazard map for Japan.

Considering the above, in this study we compile a database containing a large number of strong-motion records and then establish a base model that is able to capture the average characteristics of earthquake ground motion for PGA, PGV, and 5% damped acceleration response spectra. To improve the fit of the base model, we introduce additional correction terms for site effects and regional anomalies. Finally, a comparison with actual data and existing attenuation relations confirms that the new model is reasonably robust.

Strong Ground Motion Database

In this study, we collected all available Japanese seismic waveform data. Earthquake records from K-NET and KiK-net (Aoi *et al.*, 2000) were collected up to the 2003 Tokachi-oki earthquake and otherwise up to the end of 2002, providing a total of 91,731 records from 4967 earthquakes. Further, 788 records from 12 earthquakes in countries other than Japan were also used because the number of near-source data from large events in Japan is insufficient.

We adopted moment magnitude M_w and source distance X as the parameters for the base model. We also used the hypocenter location determined by the Japan Metrological Agency. Values of M_w were from the following references (in order of preference): (1) M_w summarized in the Fault Parameter Handbook (Sato, 1989); (2) M_w determined by F-net (Fukuyama *et al.*, 1996); (3) M_w from the CMT catalog of Harvard University; and (4) M_w converted from M_j (Japanese seismic magnitude) by a semiempirical relation (Fukushima, 1996). Further, we collected all available fault-plane models for earthquakes with M_w greater than 6.0. The source distance is the closest distance from a fault plane to the observation site and is the hypocentral distance in the case of earthquakes for which the fault model is not available. Values of M_w and the source distance for data in countries other than Japan were acquired from the Consortium of Organizations for Strong-Motion Observation Systems (COSMOS).

High-pass filtering with a cutoff frequency of 0.1 Hz was applied, while low-frequency noise was eliminated from individual nondigital records by visual inspection. The prediction parameters of our attenuation relation are horizontal peak ground acceleration, horizontal peak ground velocity, and the 5% damped horizontal acceleration response spectra. The peak value is the peak square root of the sum of squares of two orthogonal horizontal components in the time domain.

We selected data from the database for regression analysis using the following criteria: (1) M_w is not smaller than 5.5; (2) data were recorded on the ground surface; (3) two orthogonal horizontal components are available; (4) at least five stations were triggered by the event; and (5) data were truncated at an M_w-dependent source distance (Fukushima, 1997) as follows:

For PGA and response spectra:

$$f(M_w, X) < \log 10 \quad (1)$$

(data from networks including mechanical seismometer) where log represents $\log_{10}$ in the present study, and

$$f(M_w, X) < \log 2 \quad (2)$$

(data from other networks).

For PGV:

$$f(M_w, X) < \log 10 \quad (3)$$

and

$$f(M_w, X) = 0.42M_w - 0.0033X - \log(X + 0.025 \times 10^{0.42M_w}) + 1.22 \quad (4)$$

(Fukushima and Tanaka, 1992; same as Fukushima *et al.*, 2000).

Data distributions with respect to amplitude and source distance were examined for each magnitude, and those events having irregular distributions that could be associated with a particular geological/tectonic feature (such as volcanic earthquakes) were eliminated. The number of data used in the regression analysis is shown in Table 1. Data from countries other than Japan were taken from earthquakes in California, the United States, and Turkey, as shown in Table 2. These earthquakes occurred in the compressional regime and in shallow crust, matching conditions in Japan. This kind of data extension has been successfully applied by Spudich *et al.* (1997), who developed an attenuation relation applicable to Nevada by collecting worldwide strong-motion records in extensional tectonic regimes. Additionally, the 1999 Chi-Chi, Taiwan, earthquake yielded quite a lot of records. However, except very close to fault, remarkably low amplitudes are reported for this earthquake by Idriss and Abrahamson (2000), Chang *et al.* (2001), and Boore (2001). A possible explanation of these low amplitudes is that Taiwan is located on a much-fractured continental margin (Seno, 2000), and seismic wave propagation may be different than in other regions of the crust. Therefore, in this study, we excluded data from the 1999 Chi-Chi, Taiwan, earthquake from the analysis. Figure 1a and 1b shows the locations of the observation sites and earthquake epicenters used for the regression analysis, respectively. The number of observation sites in Japan and other countries totaled 2236 points and 305 points, respectively. Figure 2a and 2b shows

Table 1
Number of Data Used for Regression Analysis

	Shallow Events				Deep Events	
	Japan		Others		Japan	
Period	Data	Earthquake	Data	Earthquake	Data	Earthquake
PGA	3392	73	377	10	8150	111
5% Damped Acceleration Spectra (sec)						
0.05~1.00	3392	73	377	10	8150	111
1.10~1.20	3391	73	377	10	8145	111
1.30	3391	73	377	10	8144	111
1.50	3391	73	377	10	8140	111
1.70~2.00	3391	73	377	10	8137	111
2.20	3380	73	375	10	8100	111
2.50~3.00	3360	73	375	10	8039	110
3.50~4.00	3312	73	371	10	7963	110
4.50	3311	73	371	10	7963	110
5.00	3205	70	331	10	7721	101
PGV	2057	61	352	10	6490	110

Table 2
Earthquakes in Countries Other Than Japan Used for Regression Analysis

Source Region	Country	Origin Time (UT) (y/m/d h:m)	Focal Depth (km)	M_w
San Fernando	USA	1971/02/09 14:01	8.4	6.6
Imperial Valley	USA	1979/10/15 23:17	12.1	6.5
Morgan Hill	USA	1984/04/24 21:15	8.4	6.1
North Palm Springs	USA	1986/07/08 09:20	11.1	6.2
Whittier Narrows	USA	1987/10/01 14:42	14.7	6.1
Loma Prieta	USA	1989/10/18 00:04	17.6	7.0
Landers	USA	1992/06/28 11:58	4.5	7.3
Northridge	USA	1994/01/17 12:30	19.0	6.7
Kocaeli	Turkey	1999/08/17 00:01	17.0	7.4
Duzce	Turkey	1999/11/12 16:57	14.0	7.0

the magnitude-source distances for the PGA data used in the study, and Figure 2c shows the magnitude–focal depth distributions. The number of records from large earthquakes is relatively small and so is the number of deep events. Truncation distance increases with increasing M_w, as given in equation (4).

Regression Model

Some existing attenuation relations account for different categories of source, with earthquakes usually separated into three categories (i.e., crustal, subduction interface, and subduction intraplate events) according to their tectonic locations. Differences in strong-motion attenuation characteristics among these source categories can be expected because the different tectonic locations may lead to different source characteristics and different travel paths for the seismic waves. To take account of source effect, stress drop may be the best physical parameter. However, we were not able to include stress drop as a variable because it cannot be determined for all earthquakes in our dataset. The effect of different paths depends on focal depth to a large degree. For instance, surface waves are predominant among seismic waves generated by shallow events while this is not usually so for deep events. In Si and Midorikawa (1999), which formed the basis for the national hazard mapping project, earthquakes are divided into three categories. However, only a slight difference can be seen between crustal and subduction interface earthquakes. This fact may be due to almost the same path effect for the events of both categories, because the focal depth of the two types of events is comparatively shallower than that of slab events. Further, although several tectonic plates are subducting each other around Japan, Midorikawa and Ohtake (2002) suggested that ground-motion records from shallow and deep earthquakes had different attenuation characteristics, and the difference is due to reflection and refraction of seismic waves at Moho. We investigated the depth effect of attenuation characteristics in our database and found that ground-motion amplitudes from earthquakes with focal depths greater than 30 km are considerably different from those of shallower events. On average, the increase in amplitude saturation with decreasing distance has to be described as a function of magnitude (e.g., Campbell, 1981; Fukushima and Tanaka, 1990; Youngs *et al.*, 1997; Sadigh *et al.*, 1997) for shallow events. In our base model, we used only two parameters (moment magnitude (M_w) and source distance (X)) and two equations, one for shallow events and the other for deep events:

$$\log \text{pre} = a_1 M_w + b_1 X - \log(X + d_1 \cdot 10^{e_1 M_w}) + c_1 + \varepsilon_1 \quad (D \le 30 \text{ km}) \quad (5)$$

$$\log \text{pre} = a_2 M_w + b_2 X - \log(X) + c_2 + \varepsilon_2 \quad (D > 30 \text{ km}), \quad (6)$$

where pre is the predicted PGA (cm/sec^2), PGV (cm/sec), or 5% damped response spectral acceleration (cm/sec^2), D is the focal depth (km), and a_1, b_1, c_1, d_1, a_2, b_2, and c_2 are the regression coefficients. Takahashi *et al.* (2004) determined the coefficient of M_w in the added distance term (e_1) iteratively. Their result was about 1.1 as a natural logarithm, and this value is very close to 0.5 in the base-ten logarithmic scale. Therefore, coefficient $e_1 = 0.5$ was selected for all periods in the present study. ε_1 and ε_2 are errors between observed and predicted values. Site effects and regional features (local anomalous seismic intensity) will be considered by additional correction terms.

Regression Analysis

Method

The base model accounting for average ground-motion characteristics was determined by the two-step stratified regression analysis method of Fukushima and Tanaka (1990).

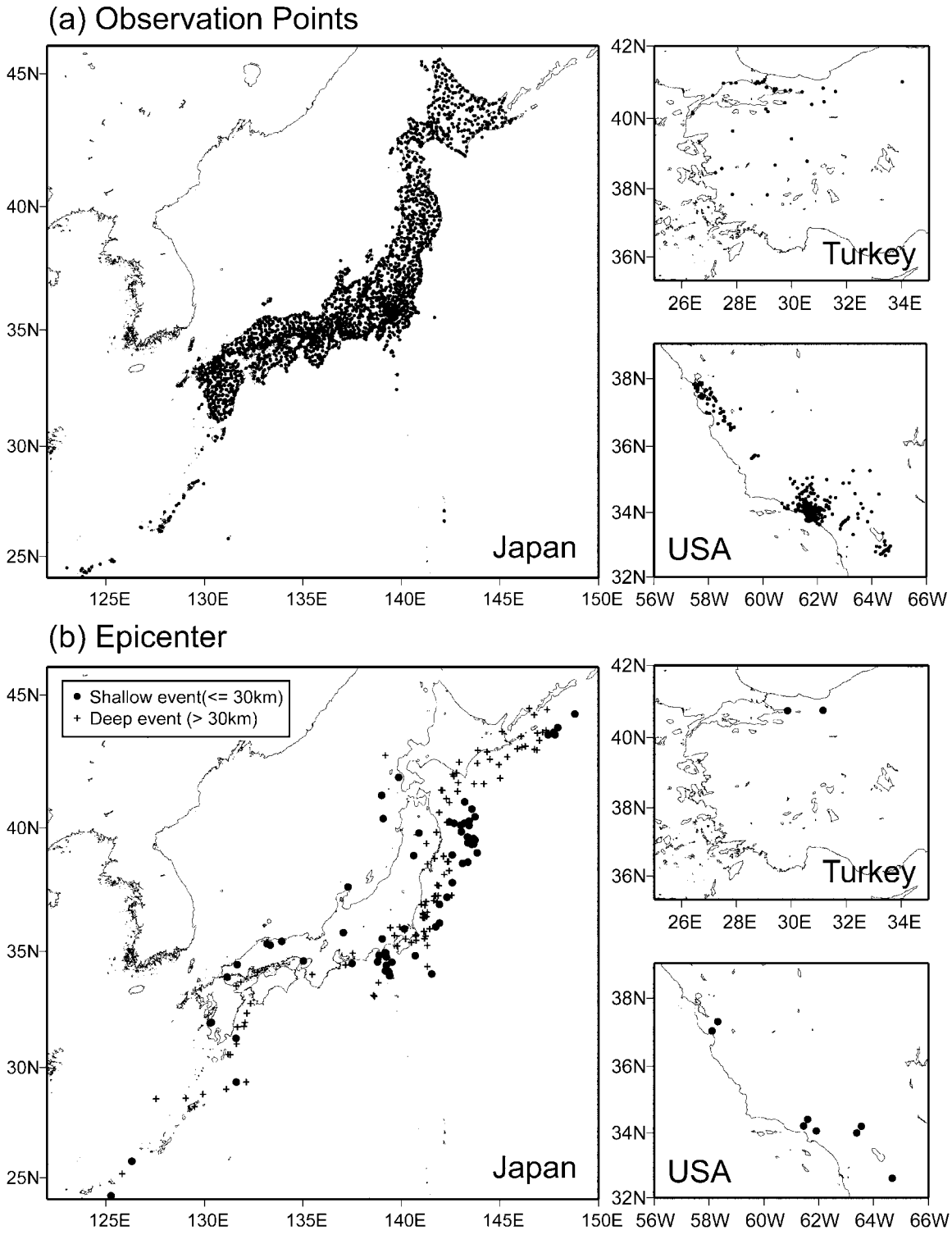

Figure 1. (a) Observation site locations and (b) epicenters of earthquakes used in regression analysis.

In the case of shallow earthquakes, an iterative procedure (Fukushima *et al.*, 2003) was applied because of the nonlinear term in equation (5). We weighted data in the near-source region to improve the near-source predictive ability of the model. The weighting scheme has no physical meaning but is a useful approach for increasing the statistical power of the near-source data. We used the same weighting scheme as adopted by Midorikawa and Ohtake (2003): 6.0 ($X \leq 25$ km), 3.0 ($25 < X \leq 50$ km), 1.5 ($50 < X \leq 75$ km), and 1.0 ($X > 75$ km).

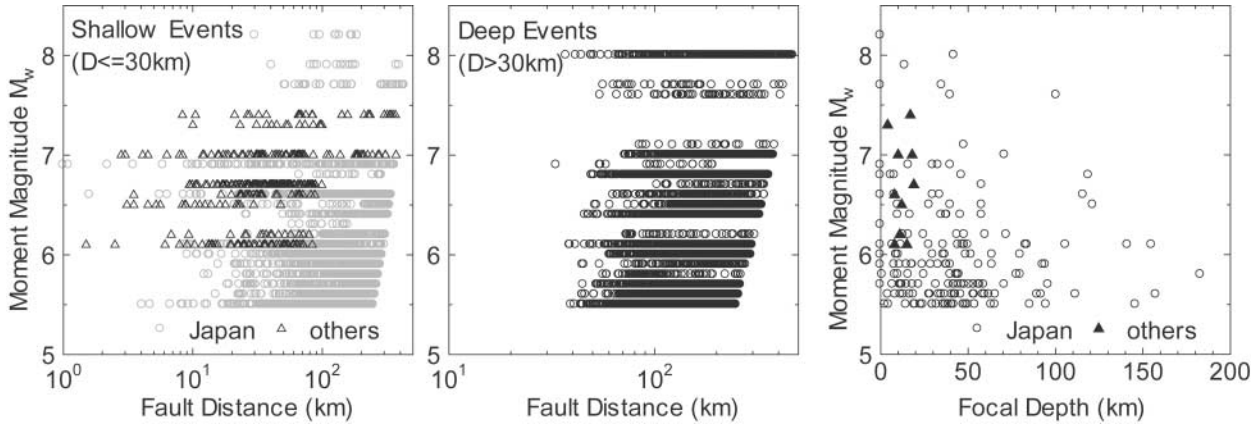

Figure 2. Magnitude–distance and magnitude–focal-depth distributions for PGA.

Results

Determined regression coefficients for the base model in equations (5) and (6) for PGA, PGV, and 5% damped response spectral acceleration are given in Tables 3 and 4 and Figure 3. Figure 4 shows PGA and PGV attenuation curves for magnitudes of 6.5, 7.0, 7.5, and 8.0. Figure 4a and b is for shallow and deep events, respectively. The magnitude dependence of PGV is stronger than that of PGA, as also found by Si and Midorikawa (1999). The attenuation rate with increasing source distance for PGA is considerably larger than that for PGV, suggesting that short-period ground motions attenuate faster than long-period ground motions. The amplitude saturation characteristics at short distance are constrained by most crustal events, although both crustal and subduction interface events fall into the category of shallow events. Therefore, the region within several tens of kilometers from the subduction interface of a large magnitude event is out of the applicable range, and predicted values for $M_w + 8.0$ and a distance of less than 20 km are indicated by dotted lines in Figure 4. Nevertheless, subduction events in Japan usually occur offshore, and prediction for close distances is not essential.

Figure 5a and b shows the predicted acceleration response spectra for shallow and deep magnitude 7.0 events, respectively. The source distances are 5, 20, 40, and 80 km for shallow events and 40, 80, 120, and 200 km for deep events. Figure 5c compares the response spectra of shallow and deep events at 40- and 80-km source distances. At long periods, the acceleration response spectra from deep earthquakes are almost the same as those from shallow events, but the short-period response spectra from deep events are much larger than those from shallow events. The difference at short periods is significant. Morikawa and Sasatani (2004) indicated extremely high stress drop for slab events in northeast Japan. A possible explanation of the significant difference at short periods is this high stress drop. Another possible reason may be the lower attenuation of high-frequency radiation in high-Q subduction zones (Youngs *et al.*, 1997).

Additional Correction Terms

Site Effects

The average shear-wave velocity at an observation station was adopted as the parameter representing site conditions. It is defined as

$$\mathrm{AVS}\,d = d \Big/ \sum_{i=1}^{n} (H_i/V_{si}), \tag{7}$$

where n is the number of strata layers down to depth d (m). H_i denotes the thickness (m) and V_{si} denotes the shear-wave velocity (m/sec) of the ith layer. Some previous studies (Matsuoka and Midorikawa, 1993; Boore *et al.*, 1997; Building Seismic Safety Council, 2000; Lussou *et al.*, 2001) have adopted $d = 30$ m; however, not all observation sites have *PS*-logging down to 30-m depth, although this is available for the KiK-net sites. On the other hand, K-NET has many observation sites with *PS*-logging down to a depth of 20 m. In order to use average shear-wave velocity at 30-m depth to represent site conditions for K-NET stations, we attempt to derive a correlation equation between AVS20 and AVS30 from the results of *PS*-logging at KiK-net sites. Figure 6 shows the almost linear correlation relationship that we used to estimate AVS30 from AVS20 for the K-NET sites. AVS30 was estimated at a total of 1081 sites among the total of 3422 sites registered in our database. The number of observation sites used to derive this additional correction term was reduced by above data selection criteria to 905 and 855 points for PGA and PGV, for example.

Zhao *et al.* (2004) used individual amplification factors for four discrete site classes. In order to obtain a continuous site correction term, we assumed the following simple equation for site effects, although predominant period dependence was eliminated:

$$G = \log(\mathrm{obs/pre}) = p \log \mathrm{AVS30} + q, \tag{8}$$

Table 3
Regression Coefficients for Shallow Event Model of PGA, PGV, and 5% Damped Acceleration Response Spectra

Period	a_1	b_1	c_1	d_1	ε_1
PGA	0.56	−0.0031	0.26	0.0055	0.37
5% Damped Acceleration Response Spectra (sec)					
0.05	0.54	−0.0035	0.48	0.0061	0.37
0.06	0.54	−0.0037	0.57	0.0065	0.38
0.07	0.53	−0.0039	0.67	0.0066	0.38
0.08	0.52	−0.0040	0.75	0.0069	0.39
0.09	0.52	−0.0041	0.80	0.0071	0.40
0.10	0.52	−0.0041	0.85	0.0073	0.40
0.11	0.50	−0.0040	0.96	0.0061	0.40
0.12	0.51	−0.0040	0.93	0.0062	0.40
0.13	0.51	−0.0039	0.91	0.0062	0.40
0.15	0.52	−0.0038	0.89	0.0060	0.41
0.17	0.53	−0.0037	0.84	0.0056	0.41
0.20	0.54	−0.0034	0.76	0.0053	0.40
0.22	0.54	−0.0032	0.73	0.0048	0.40
0.25	0.54	−0.0029	0.66	0.0044	0.40
0.30	0.56	−0.0026	0.51	0.0039	0.39
0.35	0.56	−0.0024	0.42	0.0036	0.40
0.40	0.58	−0.0021	0.26	0.0033	0.40
0.45	0.59	−0.0019	0.13	0.0030	0.41
0.50	0.59	−0.0016	0.04	0.0022	0.41
0.60	0.62	−0.0014	−0.22	0.0025	0.41
0.70	0.63	−0.0012	−0.37	0.0022	0.41
0.80	0.65	−0.0011	−0.54	0.0020	0.41
0.90	0.68	−0.0009	−0.80	0.0019	0.41
1.00	0.71	−0.0009	−1.04	0.0021	0.41
1.10	0.72	−0.0007	−1.19	0.0018	0.41
1.20	0.73	−0.0006	−1.32	0.0014	0.41
1.30	0.74	−0.0006	−1.44	0.0014	0.41
1.50	0.77	−0.0005	−1.70	0.0017	0.40
1.70	0.79	−0.0005	−1.89	0.0019	0.39
2.00	0.80	−0.0004	−2.08	0.0020	0.39
2.20	0.82	−0.0004	−2.24	0.0022	0.38
2.50	0.84	−0.0003	−2.46	0.0023	0.38
3.00	0.86	−0.0002	−2.72	0.0021	0.38
3.50	0.90	−0.0003	−2.99	0.0032	0.37
4.00	0.92	−0.0005	−3.21	0.0045	0.38
4.50	0.94	−0.0007	−3.39	0.0064	0.38
5.00	0.92	−0.0004	−3.35	0.0030	0.38
PGV	0.70	−0.0009	−1.93	0.0022	0.32

Table 4
Regression Coefficients for Deep Event Model of PGA, PGV, and 5% Damped Acceleration Response Spectra

Period	a_2	b_2	c_2	ε_2
PGA	0.41	−0.0039	1.56	0.40
5% Damped Acceleration Response Spectra (sec)				
0.05	0.39	−0.0040	1.76	0.42
0.06	0.39	−0.0041	1.86	0.43
0.07	0.38	−0.0042	1.96	0.45
0.08	0.38	−0.0042	2.03	0.45
0.09	0.38	−0.0043	2.08	0.46
0.10	0.38	−0.0043	2.12	0.46
0.11	0.38	−0.0044	2.14	0.46
0.12	0.38	−0.0044	2.14	0.46
0.13	0.38	−0.0044	2.13	0.46
0.15	0.39	−0.0044	2.12	0.46
0.17	0.40	−0.0043	2.08	0.45
0.20	0.40	−0.0042	2.02	0.44
0.22	0.40	−0.0041	1.99	0.43
0.25	0.41	−0.0040	1.88	0.42
0.30	0.43	−0.0038	1.75	0.42
0.35	0.43	−0.0036	1.62	0.41
0.40	0.45	−0.0034	1.49	0.41
0.45	0.46	−0.0032	1.33	0.41
0.50	0.47	−0.0030	1.19	0.40
0.60	0.49	−0.0028	0.95	0.40
0.70	0.51	−0.0026	0.72	0.40
0.80	0.53	−0.0025	0.49	0.40
0.90	0.56	−0.0023	0.27	0.40
1.00	0.57	−0.0022	0.08	0.41
1.10	0.59	−0.0022	−0.08	0.41
1.20	0.60	−0.0021	−0.24	0.41
1.30	0.62	−0.0020	−0.40	0.41
1.50	0.64	−0.0020	−0.63	0.41
1.70	0.66	−0.0018	−0.83	0.40
2.00	0.68	−0.0017	−1.12	0.40
2.20	0.69	−0.0017	−1.27	0.40
2.50	0.71	−0.0017	−1.48	0.39
3.00	0.73	−0.0017	−1.72	0.39
3.50	0.75	−0.0017	−1.97	0.38
4.00	0.77	−0.0016	−2.22	0.37
4.50	0.79	−0.0016	−2.45	0.36
5.00	0.82	−0.0017	−2.70	0.35
PGV	0.55	−0.0032	−0.57	0.36

where G is an additional correction term corresponding to site effects and log(obs/pre) is the residual between the observed amplitude of PGA, PGV, and spectral acceleration (obs) and the values predicted (pre) by the base model in equations (5) and (6). Coefficients p and q were derived by regression analysis on the residuals averaged at intervals of every 100 m/sec in AVS30. The predicted value after applying the additional correction terms corresponding to site effects (pre_G) can be simply interpreted as follows:

$$\log \mathrm{pre}_G = \log \mathrm{pre} + G. \quad (9)$$

Figure 7 shows, as examples, the relations between averaged residuals and AVS30 for PGA and PGV, while Table 5 presents the coefficients for equation (8). A considerable decrease of the averaged residuals with increasing AVS30 can be seen in the figure.

Figure 8a shows absolute values of correlation coefficients between model residuals and AVS30. Statistical tendency of the additional site effect correction increases with the correlation coefficients. We can see enough high value of the cross-correlation, so equation (8) can be applied to wide AVS30 range. However the correlation coefficient at around 0.1 sec is smaller than that at other period ranges. A possible explanation of this dip is that site amplification effects at short periods may be the second or higher mode responses of soil sites. The second modal period of a soil site is approximately the natural period divided by 2.5–3.0

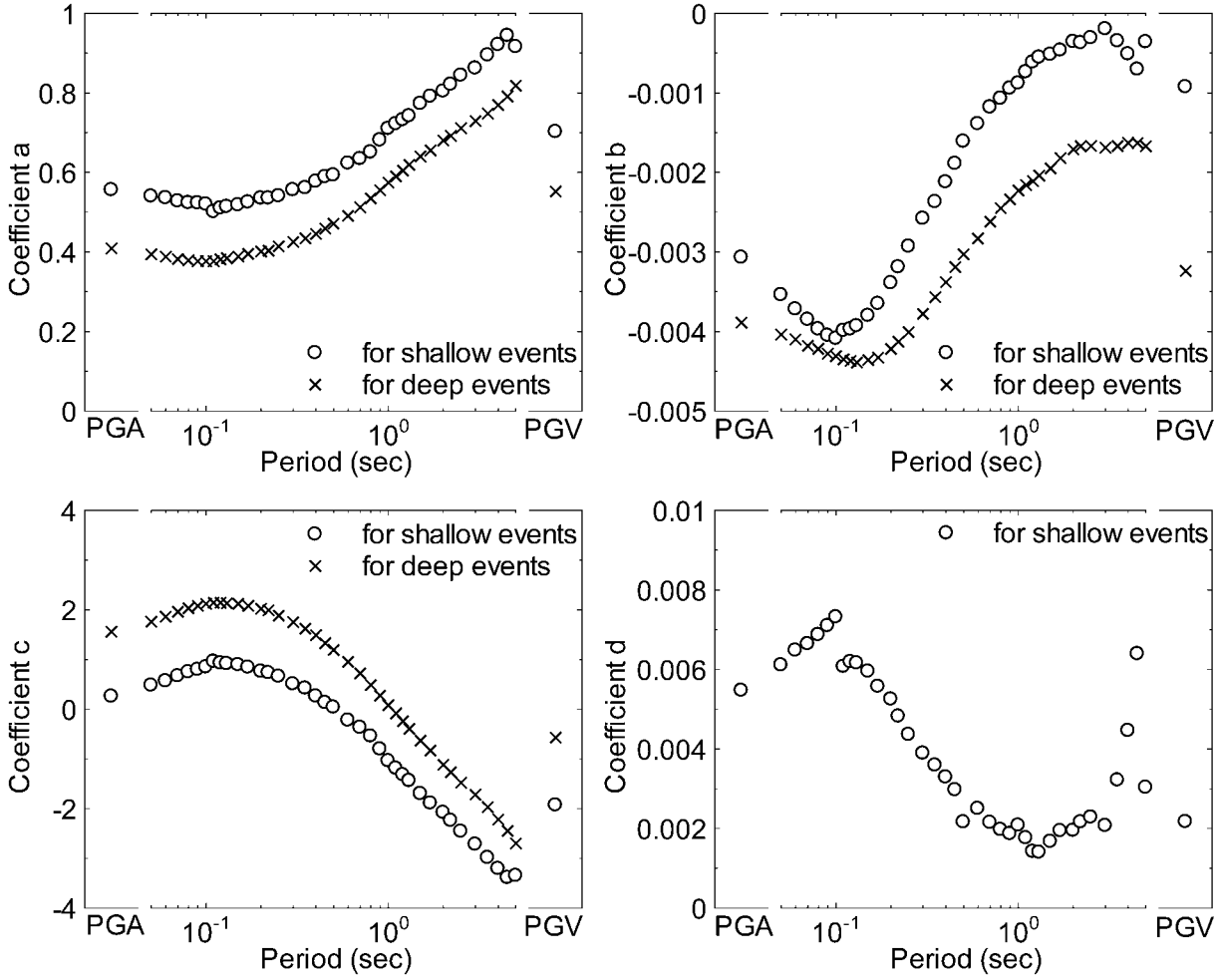

Figure 3. Regression coefficients for PGA, PGV, and 5% damped acceleration response spectra in equations (5) and (6).

for a soil layer with a uniform or moderately increasing shear-wave velocity with increasing depth, while the third modal period is approximately the natural period divided by 4.0–5.0. This leads to the possibility that ground motion at 0.1 sec may be related to the second mode for a site with a natural period of 0.3 sec and the third mode for a site with a natural period of 0.4 sec or longer. However, the period and amplification ratio of the second or higher mode would depend on the precise variation of soil shear-wave velocity with depth, which is not easily represented by AVS30. It is also possible that moderate nonlinear soil deformation at a soft soil site might considerably alter the amplification ratios at short periods, though only a small number of records in our dataset are large enough to induce nonlinear soil deformation.

Further, the stability of the correction function was investigated by looking at the zero-crossing points of equation (8). Although the equation was determined from averaged residuals for individual intervals in AVS30, the zero-crossing point should be at approximately 300 m/sec of predominant in our database, whatever the period range. Actually, in Figure 8b, AVS30 values of the zero-cross points are concentrated around 300 m/sec.

Figure 8c shows coefficient p in equation (8), which corresponds to the shear-wave velocity dependence of site amplification. This dependence is generally greater than determined by Midorikawa *et al.* (1994) and Boore *et al.* (1997), but the pattern of variation with period is very similar to these earlier results, including the trough at a period of around 1 sec.

Figure 9 shows how the standard deviation decreases after introducing the site correction terms. Although this reduction in standard deviation can be seen in almost every period range, the standard deviation decreases only slightly in the short-period range ($<$0.2 sec). On the other hand, the standard deviation decreases considerably at a period of around 1 sec. In this period range, a significant dip in p value can be seen in Figure 8c, meaning that the residuals strongly depend on AVS30. This demonstrates that the proposed correction is very effective around this period.

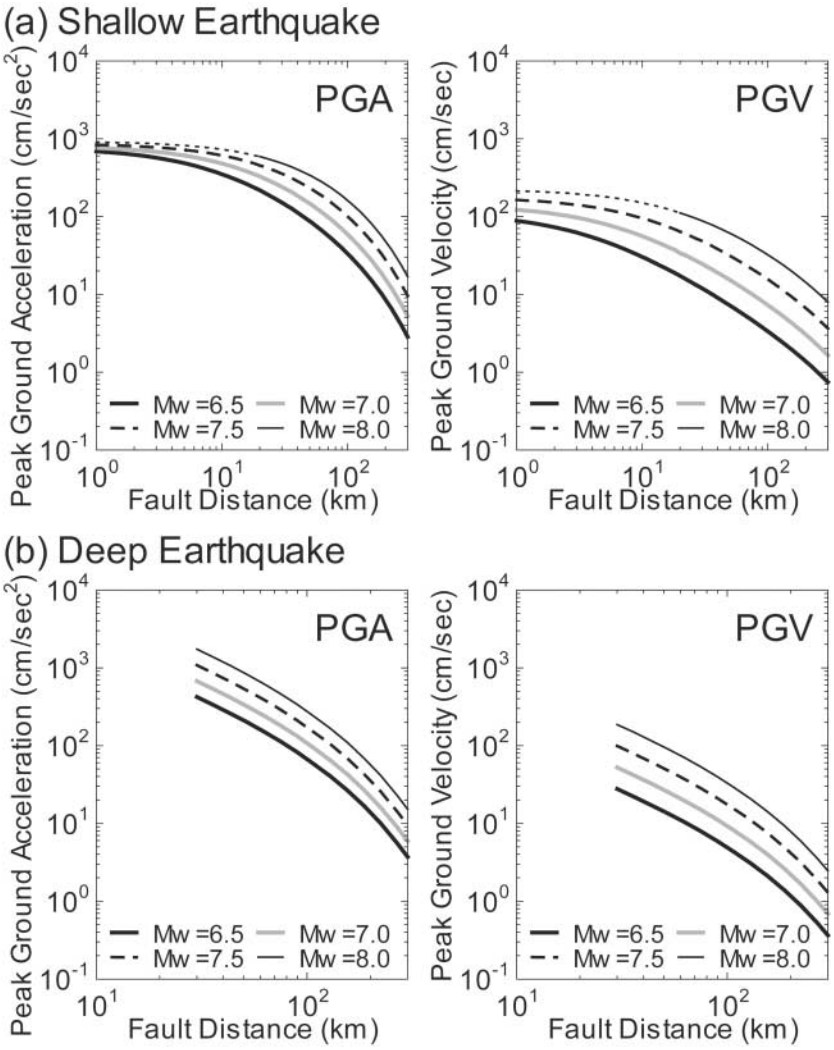

Figure 4. Attenuation curves of PGA and PGV for M_w 6.5, 7.0, 7.5, and 8.0: (a) shallow earthquake; (b) deep earthquake.

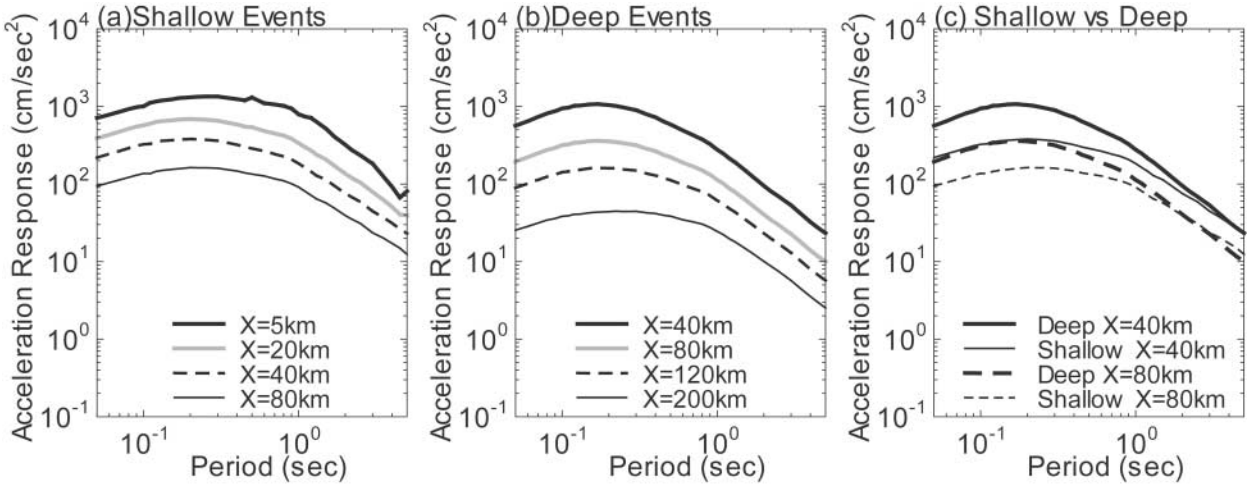

Figure 5. Predicted acceleration response spectra for magnitude 7.0 (a) for shallow and (b) deep events at representative source distances, and (c) a comparison of the response spectra between shallow and deep events at 40 and 80 km source distances.

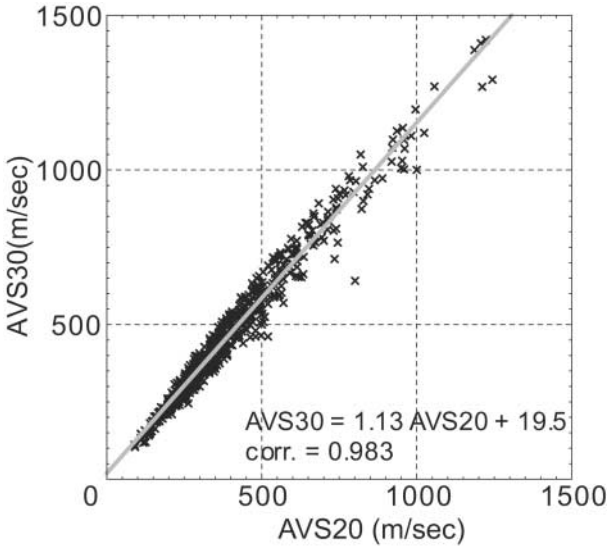

Figure 6. Relationship between AVS20 and AVS30.

Anomalous Seismic Intensity in Northeast Japan

Intermediate and deep earthquakes occurring in the Pacific plate usually generate anomalous seismic intensity in Japan's northeast. This anomalous seismic intensity is a large-scale abnormal distribution of relatively larger ground motions that cannot be explained by source or site effects. These anomalous larger ground motions have been observed more commonly in fore-arc side (south or east of volcanoes) than in back-arc side (north or west of volcanoes; Figure 10a). This phenomenon is explained by a unique Q structure beneath the island-arc region shown in Figure 10c (Utsu, 1967). Namely, seismic waves to a fore-arc propagate shorter in low-Q zone than those to a back-arc. Actually, a considerable contrast in Q is expected; it is about 300 or less and 1500 or more for low Q and high Q, respectively (e.g., Umino and Hasegawa, 1984). In order to accommodate this regional anomaly, Morikawa *et al.* (2003) proposed additional correction terms for the attenuation relations given by Si and Midorikawa (1999). Our analysis reveals similar bias, and we also introduce the additional correction terms to the base model plus the site correction terms described in the last section. The procedure is the same as that of Morikawa *et al.* (2003), which is a depth correction term defined by

$$A = \log(\text{obs/pre}) = (\alpha \cdot R_{\text{tr}} + \beta) \cdot (D - 30), \quad (10)$$

where A is additional correction term corresponding to anomalous seismic intensity, and α and β are the regression coefficients. R_{tr} is the shortest distance from the observation site to the Kuril, Japan, and Izu-Bonin trenches, as shown in Figure 10; that is, the shortest distance from the site to the trench axis. A subdataset for this depth correction is extracted from among deep earthquakes (30 km or deeper) satisfying the following criteria: (1) hypocenters located in the Pacific plate; (2) observation sites located to the east of 137° longitude east; and (3) observation sites provide estimated AVS30. The formulation of equation (10) is able to qualitatively explain the characteristics of seismic-wave attenuations caused by the unique Q structure beneath northeast Japan as shown inFigure 10c. For deeper events, amplitudes in the fore-arc (with small R_{tr}) region become larger as seismic waves propagate long distances within a high Q slab, while amplitudes on the back-arc side of the volcanic front (with large R_{tr}) are smaller due to seismic waves propagating long distances within the underlying low Q mantle wedge.

The predicted value after applying the additional correction terms corresponding to anomalous seismic intensity (pre_A) can be also interpreted as

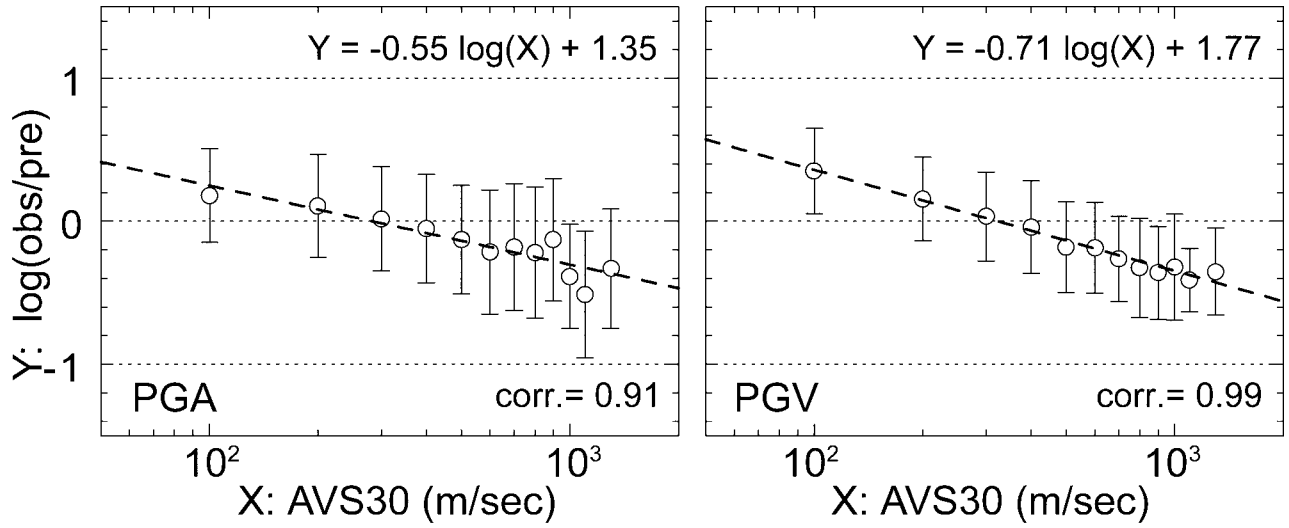

Figure 7. Relationship between residual and AVS30 for PGA and PGV.

Table 5
Obtained Coefficients in Equation (8)

Period	p	q
PGA	−0.55	1.35
5% Damped Acceleration Response Spectra (sec)		
0.05	−0.32	0.80
0.06	−0.26	0.65
0.07	−0.24	0.60
0.08	−0.26	0.64
0.09	−0.29	0.72
0.10	−0.32	0.78
0.11	−0.35	0.84
0.12	−0.39	0.94
0.13	−0.43	1.04
0.15	−0.53	1.28
0.17	−0.61	1.47
0.20	−0.68	1.65
0.22	−0.72	1.74
0.25	−0.75	1.82
0.30	−0.80	1.96
0.35	−0.85	2.09
0.40	−0.87	2.13
0.45	−0.89	2.18
0.50	−0.91	2.25
0.60	−0.92	2.30
0.70	−0.96	2.41
0.80	−0.98	2.46
0.90	−0.97	2.44
1.00	−0.93	2.32
1.10	−0.92	2.30
1.20	−0.91	2.26
1.30	−0.88	2.20
1.50	−0.85	2.12
1.70	−0.83	2.06
2.00	−0.78	1.92
2.20	−0.76	1.88
2.50	−0.72	1.80
3.00	−0.68	1.70
3.50	−0.66	1.64
4.00	−0.62	1.54
4.50	−0.60	1.50
5.00	−0.59	1.46
PGV	−0.71	1.77

$$\log \mathrm{pre}_A = \log \mathrm{pre} + A. \quad (11)$$

Estimates of the coefficients in equation (10) are given in Table 6. Figure 11 shows the standard deviations with and without the correction terms in equation (10). For PGA and the response spectra at short periods, the reduction in standard deviation is considerably large. However, the correction term has relatively little effect on PGV and response spectra with a period beyond 0.6 sec. This finding agrees with the results obtained by Maeda and Sasatani (2002), who suggested that the difference in Q value between fore- and back-arc sides (where a high Q value may cause anomalous seismic intensity) was not significant for periods over 1 sec.

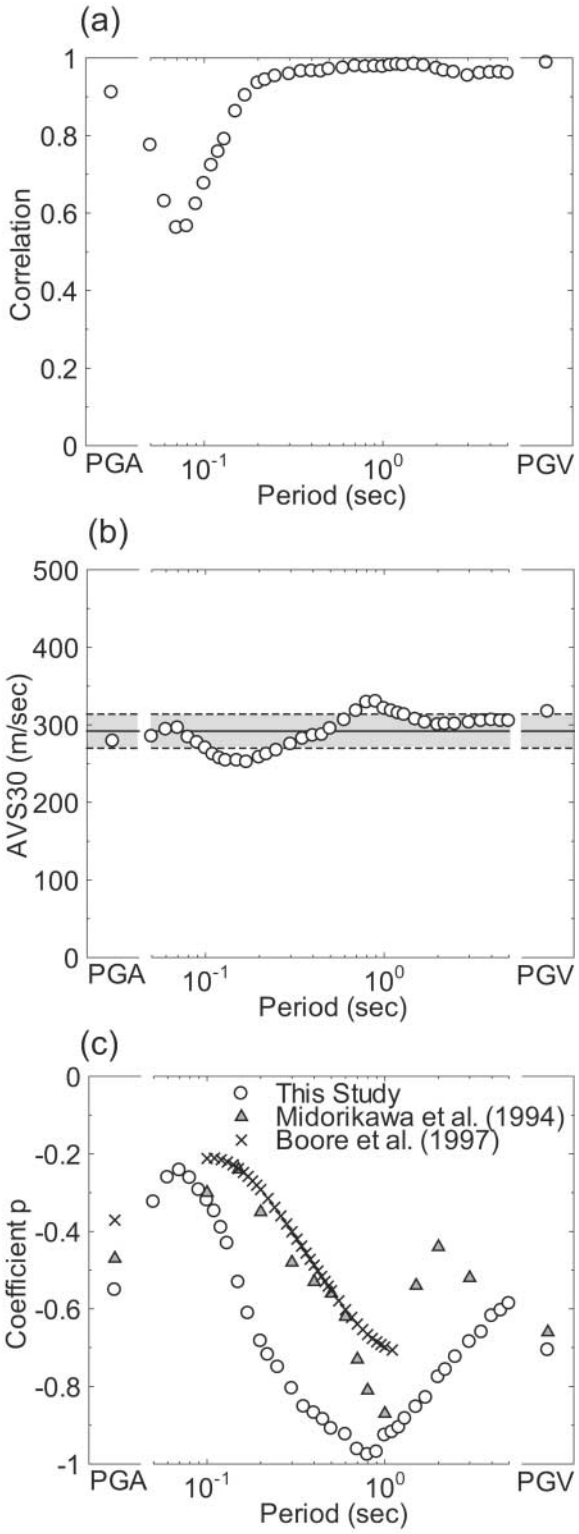

Figure 8. (a) Correlation coefficients between residual and AVS30. (b) AVS30 at the zero-crossing point of equation (8) for the individual period. Solid line indicates overall average and shaded band indicates the standard deviation. (c) Coefficient p of equation (8) corresponding to dependence of AVS30.

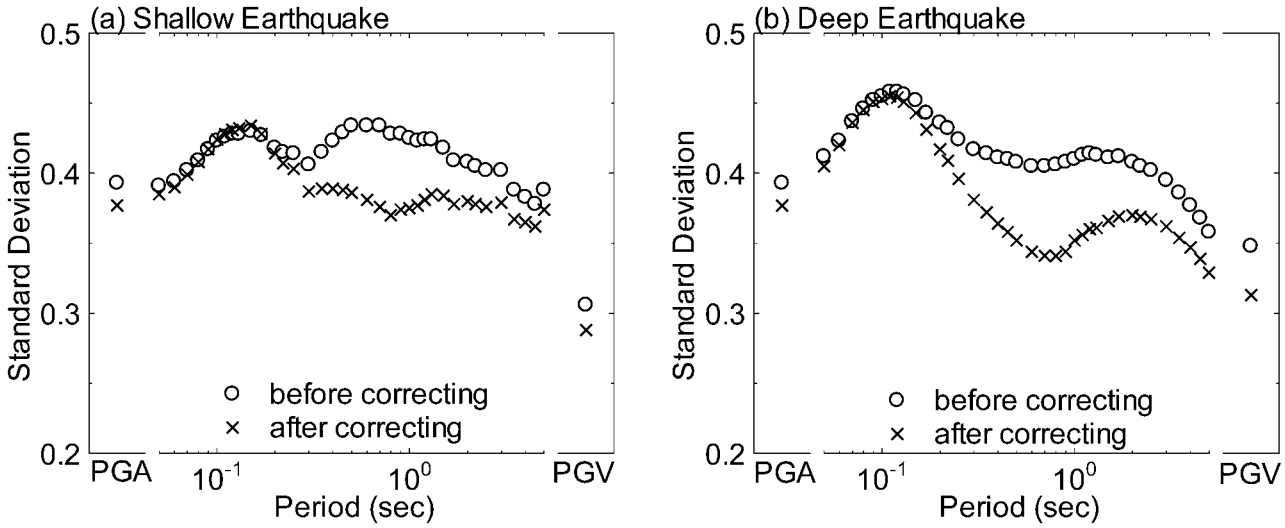

Figure 9. Standard deviations before and after applying the additional correction terms corresponding to site effects: (a) shallow earthquake; (b) deep earthquake.

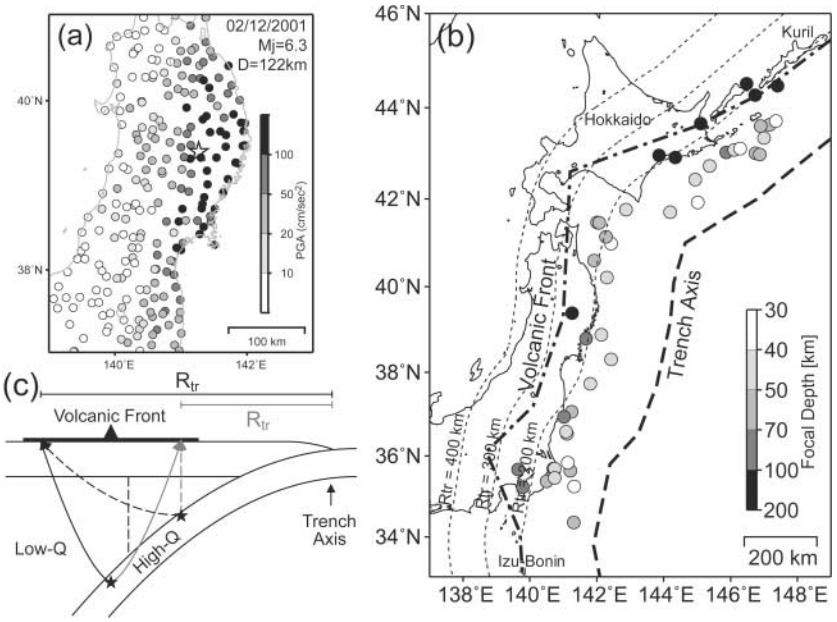

Figure 10. (a) Example of anomalous seismic intensity in northeast Japan; (b) epicenters of data used for estimating the additional correction terms for anomalous seismic intensity in northeast Japan. Broken line is the trench axis. (c) Schematic illustration of the unique Q structure beneath northeast Japan and ray paths for intermediate-depth earthquakes (Morikawa *et al.*, 2003).

Discussion

Comparison with Existing Attenuation Relations

Figure 12 compares ground motions predicted by our model with existing models. In this figure, FT92, BJF97, AYK97, SM99, and MO02 denote Fukushima and Tanaka (1992), Boore *et al.* (1997), Annaka *et al.* (1997), Si and Midorikawa (1999), and Midorikawa and Ohtake (2002), respectively. Magnitude M_w 7.0 was used in all cases because damage often occurs in Japan when the magnitude exceeds 7. A focal depth $D = 10$ km was used for shallow crustal earthquakes and $D = 60$ km was used for deep intraplate earthquakes. These depths are the average values in our database. The site conditions for PGA and PGV were assumed to be 300 and 600 m/sec for soil and rock, respectively, corresponding to the models of Si and Midorikawa (1999) and Midorikawa and Ohtake (2002).

The PGA values predicted for shallow events by our model are similar to those predicted by the other models. On the contrary, PGV values predicted for shallow events by our model bend more gently in the near-source region than others, and the amplitude is almost 2 times larger than that of Annaka *et al.* (1997). The attenuation characteristics of predicted PGA and PGV for deep events agree well with the

Table 6
Obtained Coefficients in Equation (10)

Period	α	β
PGA	-6.73×10^{-5}	2.09×10^{-2}
5% Damped Acceleration Response Spectra (sec)		
0.05	-7.78×10^{-5}	2.37×10^{-2}
0.06	-8.02×10^{-5}	2.42×10^{-2}
0.07	-8.15×10^{-5}	2.47×10^{-2}
0.08	-8.22×10^{-5}	2.50×10^{-2}
0.09	-8.26×10^{-5}	2.55×10^{-2}
0.10	-8.23×10^{-5}	2.54×10^{-2}
0.11	-8.18×10^{-5}	2.56×10^{-2}
0.12	-8.08×10^{-5}	2.53×10^{-2}
0.13	-7.99×10^{-5}	2.51×10^{-2}
0.15	-7.99×10^{-5}	2.51×10^{-2}
0.17	-7.53×10^{-5}	2.38×10^{-2}
0.20	-6.99×10^{-5}	2.23×10^{-2}
0.22	-6.54×10^{-5}	2.09×10^{-2}
0.25	-6.07×10^{-5}	1.96×10^{-2}
0.30	-5.47×10^{-5}	1.78×10^{-2}
0.35	-5.06×10^{-5}	1.67×10^{-2}
0.40	-4.62×10^{-5}	1.54×10^{-2}
0.45	-4.62×10^{-5}	1.51×10^{-2}
0.50	-4.41×10^{-5}	1.44×10^{-2}
0.60	-3.60×10^{-5}	1.19×10^{-2}
0.70	-2.88×10^{-5}	9.48×10^{-3}
0.80	-2.50×10^{-5}	8.19×10^{-3}
0.90	-2.16×10^{-5}	7.35×10^{-3}
1.00	-2.18×10^{-5}	7.61×10^{-3}
1.10	-1.95×10^{-5}	7.08×10^{-3}
1.20	-1.63×10^{-5}	6.52×10^{-3}
1.30	-1.38×10^{-5}	5.85×10^{-3}
1.50	-1.18×10^{-5}	5.52×10^{-3}
1.70	-8.53×10^{-6}	4.80×10^{-3}
2.00	-4.53×10^{-6}	4.05×10^{-3}
2.20	-1.18×10^{-6}	3.11×10^{-3}
2.50	2.60×10^{-6}	2.15×10^{-3}
3.00	3.01×10^{-6}	2.01×10^{-3}
3.50	2.49×10^{-6}	2.06×10^{-3}
4.00	9.28×10^{-6}	2.27×10^{-3}
4.50	-2.13×10^{-6}	2.95×10^{-3}
5.00	-4.61×10^{-6}	3.44×10^{-3}
PGV	-1.94×10^{-5}	7.24×10^{-3}

Midorikawa and Ohtake (2002) model, which took account of the different attenuation rates for shallow and deep events. However, the predicted PGV is almost same as the Midorikawa and Ohtake (2002) value and about 1.5 times larger than that predicted by Si and Midorikawa (1999) or Annaka *et al.* (1997) at a source distance of 50 km. Spectral accelerations for shallow events predicted by our model agree reasonably well with those predicted by others. However, for short periods less than 0.4 sec, spectral accelerations predicted by our model for deep events are much lager than those predicted by the Annaka *et al.* (1997) model. This large difference may be a result of using very different databases.

Comparison with Observed Records and Residuals of the New Attenuation Models

Figure 13 compares values predicted using the attenuation models developed in this study with corresponding values calculated from the records. Note that site correction terms have been incorporated for both shallow and deep events, and the depth correction terms have also been used in the model for deep events in the northeast of Japan. Figure 13a and b shows a comparison of attenuation curves obtained in the present study with data normalized to M_w 7.0, D = 10 km, and AVS30 = 300 m/sec (soil) from shallow earthquakes. The observed data were normalized as follows:

$$\log \text{obs}' = \log \text{obs} - \log \text{pre}_{\text{all}} + \log \text{pre}'_{\text{all}}, \quad (12)$$

where obs′ is the normalized data, pre_{all} is the predicted value for identical parameters with observed data, and pre'_{all} is the predicted value under the normalization conditions (Fukushima *et al.*, 2003). The PGA and PGV values close to the source fault are around 750 cm/sec^2 and 80 cm/sec, respectively. Figure 13c and d compare data for deep events. These data were normalized to D = 60 km and R_{tr} without the influence of the anomalous seismic intensity, while the other normalization parameters are the same as those for the shallow events. The attenuation model for deep events fits the data very well at all distances.

Distributions of total residuals between observed and predicted PGAs and PGVs (log (obs/pre)) with respect to source distance and predicted values are shown in Figure 14. The residuals decrease with increasing predicted amplitude and with decreasing source distance. These residual distributions suggest that PGAs and PGVs at short distance and large amplitudes can be better estimated by our model than those at long distance and small amplitude, and this is a desirable property for engineering applications. Although this property is also indicated by Midorikawa and Ohtaka (2003), it may result not from the modeling, but from the lack of sufficient data for these amplitude and distance ranges

Figure 15 shows the distribution of total, intraevent, and interevent residuals with respect to focal depth for events with a focal depth larger than 30 km. Figure 15a is for PGA. The first row of plots in Figure 15a show that, with no correction terms at all, the intraevent residuals are not biased with focal depth but the interevent residuals are. The mean values of total error increase with focal depth up to 70 km and then appear to be constant for deeper events. The bias in the total error distribution is largely from interevent residuals. The second row in Figure 15a shows that the depth correction terms have reduced the intraevent residuals considerably but the interevent error has increased slightly; the bias with respect to focal depth has improved for most events within a focal depth of 140 km. The correction for the three deepest events appears to be too severe, leading to a slight

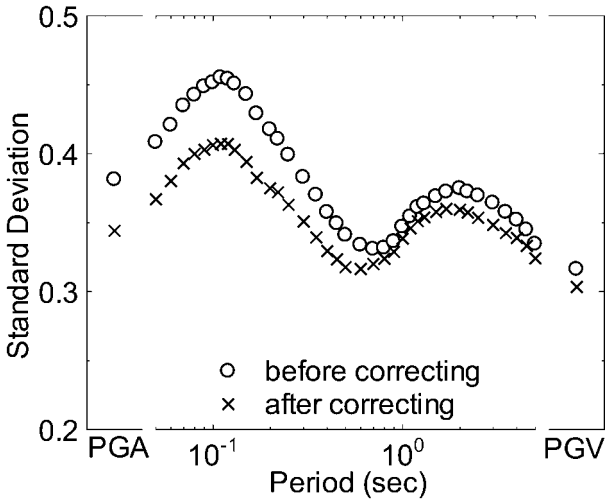

Figure 11. Standard deviations before and after applying the additional correction terms corresponding to anomalous seismic intensity in northeast Japan.

increase in interevent standard deviation. Residuals in the third row of Figure 15a show that the correction term for site conditions has a marginal effect on PGA, with intraevent error being reduced to 0.27 from 0.28 while the interevent error increases slightly. We expect stress drop to increase with increasing focal depth for deep events and anticipate that this effect can be accounted for by the depth term in our correction term.

Interevent errors for events deeper than 140 km decrease with increasing focal depth after applying correction factors to accommodate the anomalous seismic intensity. For most periods, the correction factor of equation (10) is zero when R_{tr} is about 300 km, positive for $R_{tr} < 300$ km, and negative for $R_{tr} > 300$ km. Therefore, the correction term amplifies the spectra at sites on the fore-arc side where $R_{tr} < 300$ km, while those at sites on the back-arc side, where $R_{tr} > 300$ km, are attenuated. On the other hand, we implicitly assumed in equation (10) that the trench axis parallels the volcanic front.

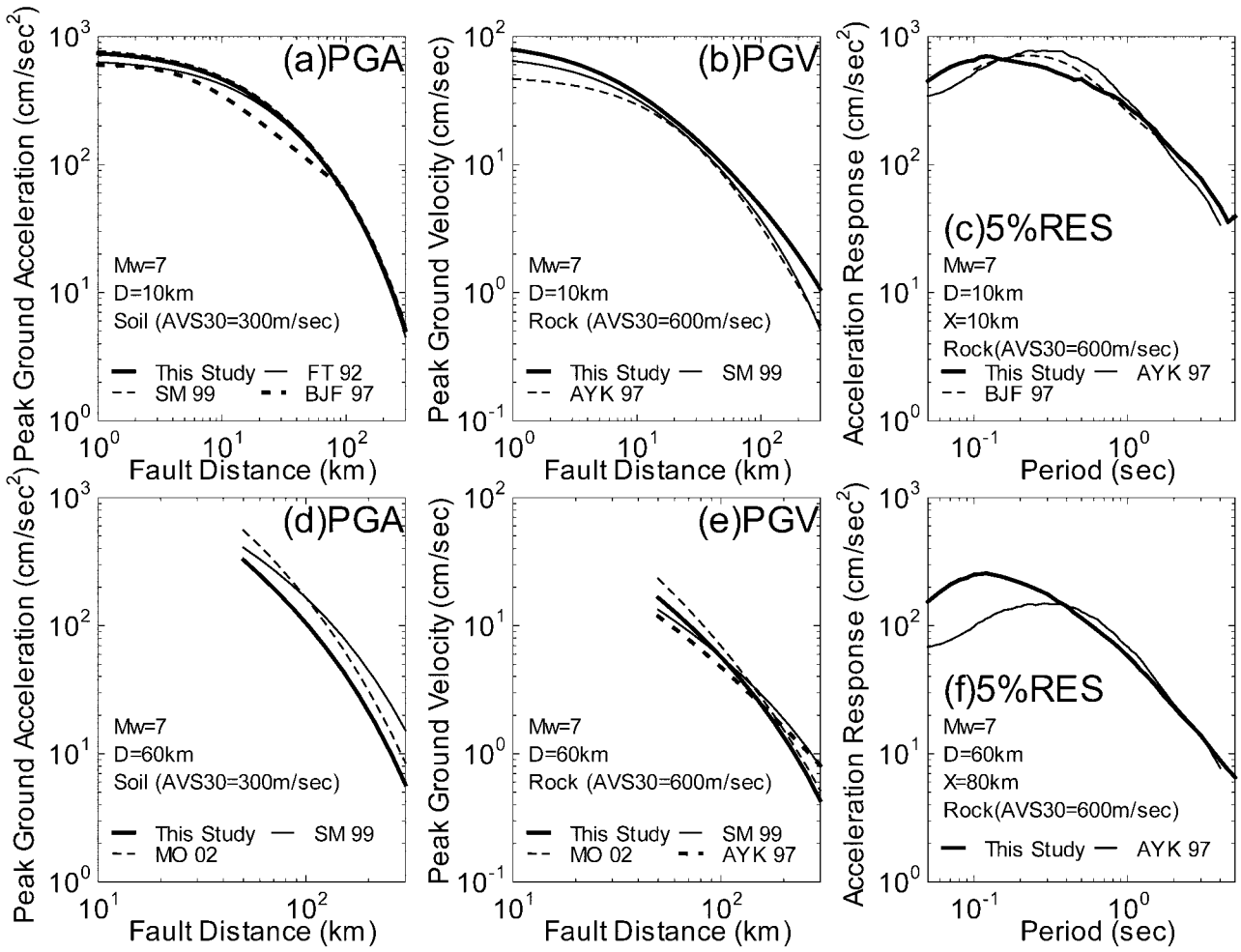

Figure 12. Comparison of new attenuation curves with others: FT92, SM99, BJF97, AYK99, and MO02 are Fukushima and Tanaka (1992), Si and Midorikawa (1999), Boore *et al.* (1997), Annaka *et al.* (1997), and Midorikawa and Ohtake (2002), respectively.

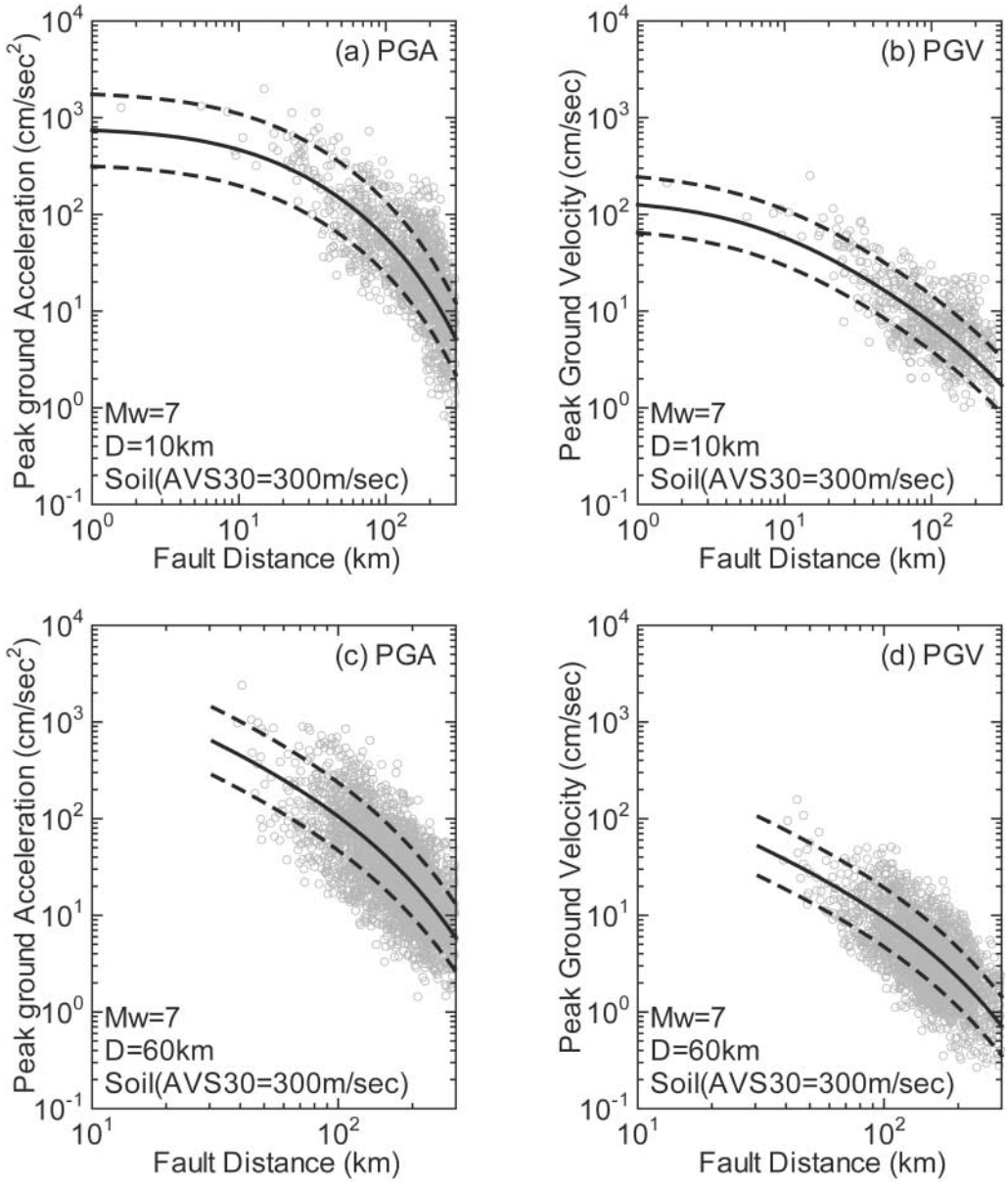

Figure 13. Comparison of attenuation curves obtained in this study with normalized data. Data are normalized to M_w 7.0, D = 10 km, and AVS30 = 300 m/sec (soil) for shallow events. Normalization parameters for deep events are D = 60 km and R_{tr} without influence of anomalous seismic intensity, while others are the same as those for shallow events. Solid and broken lines are the new attenuation curves and standard deviations.

The distance between the volcanic front and the trench axis decreases in the eastern Hokkaido, southern Kuril, and Izu-Bonin regions (Fig. 10a). For this part of Japan, equation (10) enhances the predicted response spectra when $R_{tr} <$ 300 km but the seismic waves reaching these sites have been attenuated (passing the low Q mantle wedge), leading to overestimations of spectra in the eastern part of Hokkaido and Izu-Bonin islands. In our database, all strong-motion data for earthquakes deeper than 140 km are from the eastern part of Hokkaido, and the overestimation of spectra for these events by equation (10) leads to an apparent bias in inter-event errors for events with a focal depth of 140 km or more shown in Figure 15a. This result may suggest that we should use other parameters instead of R_{tr}.

Figure 15b is for the 5% damped response acceleration of 1-sec period. In contrast to the case of PGA, where the site correction terms lead to minimal reduction in total and intraevent error, the site correction terms at 1 sec lead to significant reduction of intraevent errors (from 0.33 to 0.27) and total errors (from 0.40 to 0.35). Note that the anomalous

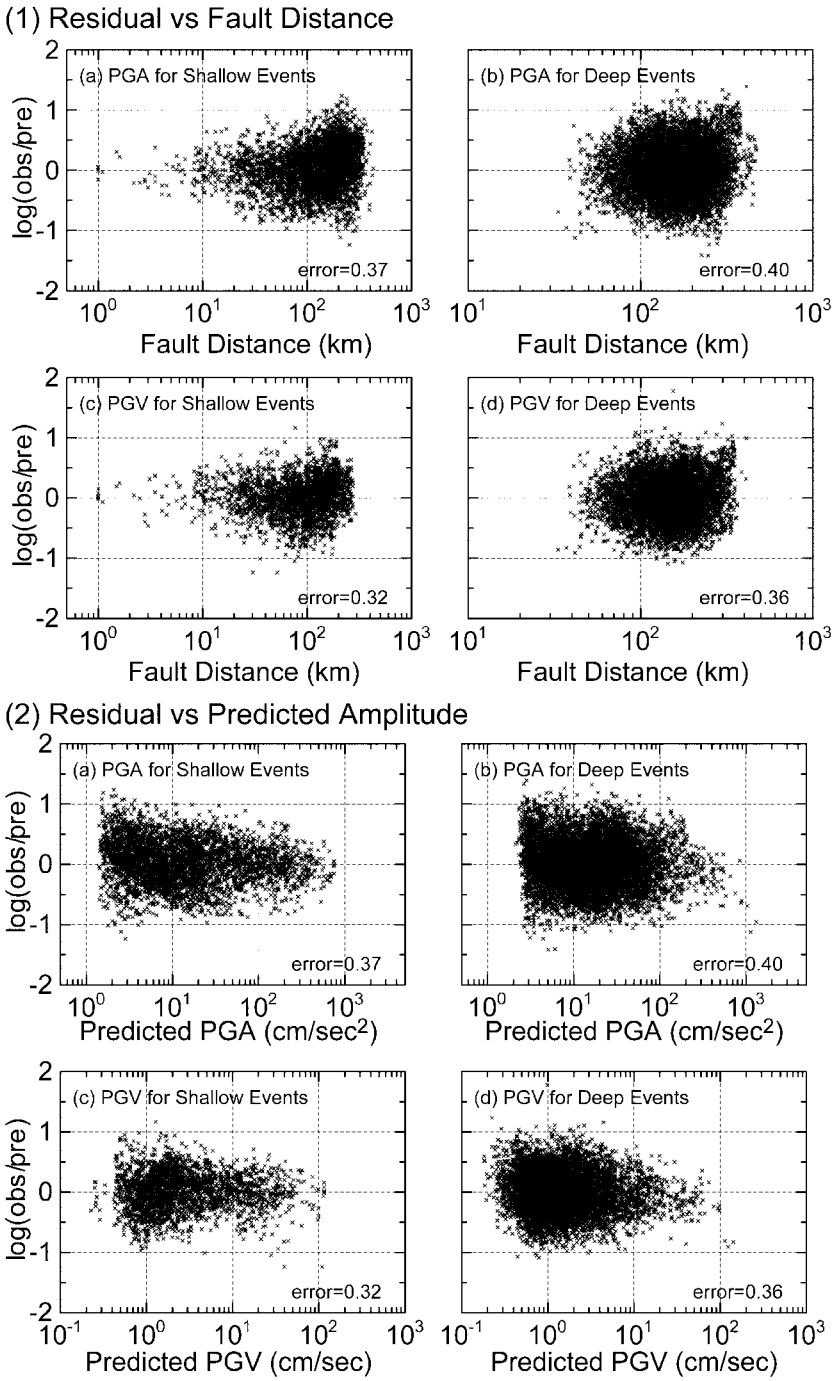

Figure 14. Relationship between residuals and (1) fault distance and (2) predicted amplitude. "Error" in these figures means total error between observed and predicted values.

seismic intensity correction terms produce a marginal reduction in intraevent errors at long periods, as expected.

Figure 16 shows the distribution of PGA residuals with respect to moment magnitude. There is no bias in total, intraevent, and interevent errors.

Conclusions

We collected all available Japanese seismic waveform data, including those from the many strong-motion observation stations set up by the Japanese government and other organizations, and used them to establish a new database. A large number of high-quality strong-motion records were obtained from these new networks. Based on the new database, we proposed new standard attenuation relations not only for peak values, such as PGA and PGV, but also for 5% damped acceleration response spectra, as a contribution to a future national seismic hazard map of Japan. The conclusions of the study can be summarized as follows:

- We assembled the largest possible number of seismic waveforms, obtaining a total of 91,731 records from 4967

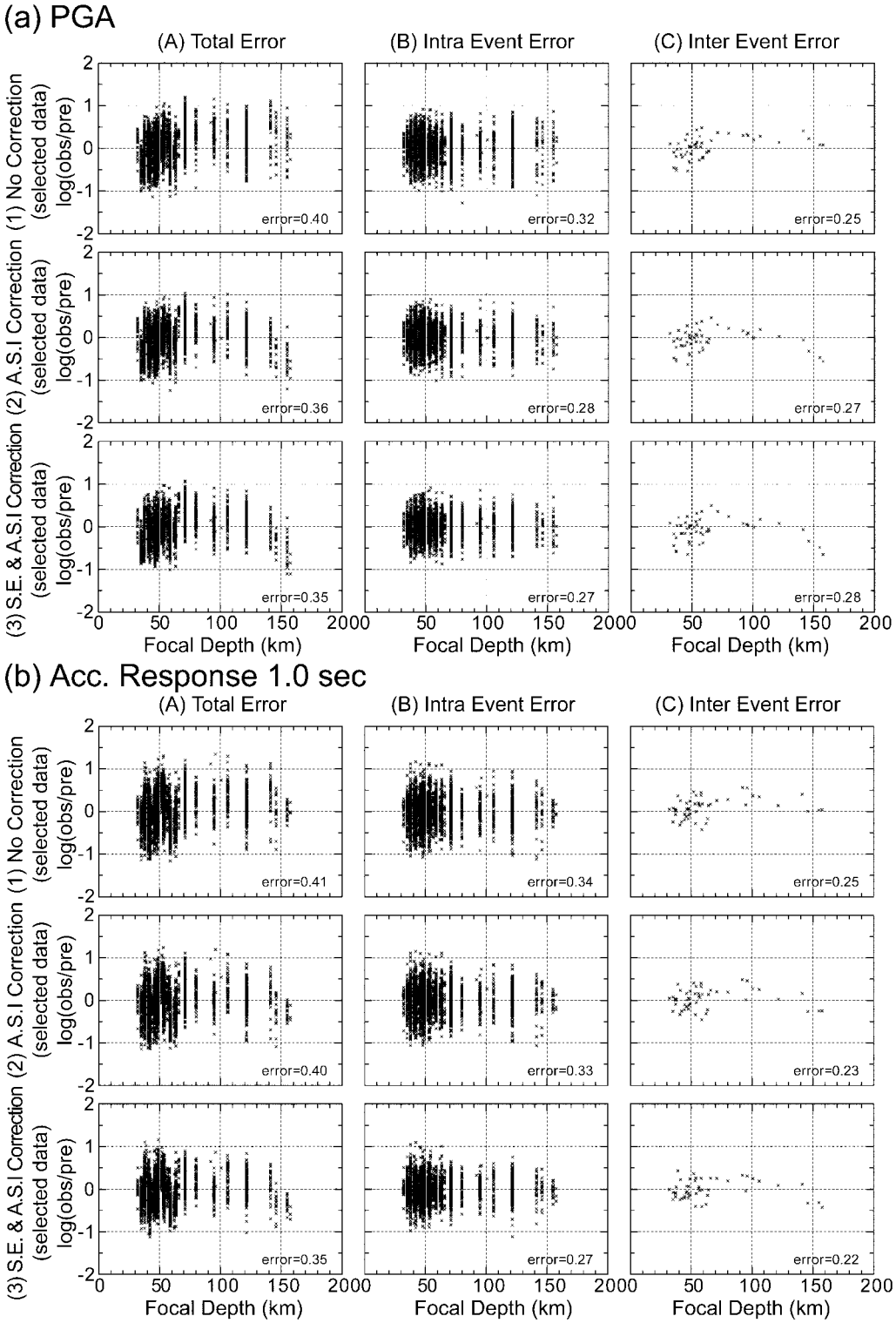

Figure 15. Relationship between residual and focal depth for (a) PGA and (b) 5% damped acceleration response of 1-sec period for deep events. Data that can be corrected for site effects (S.E.) and anomalous seismic intensity in northeast Japan (A.S.I.) are selected.

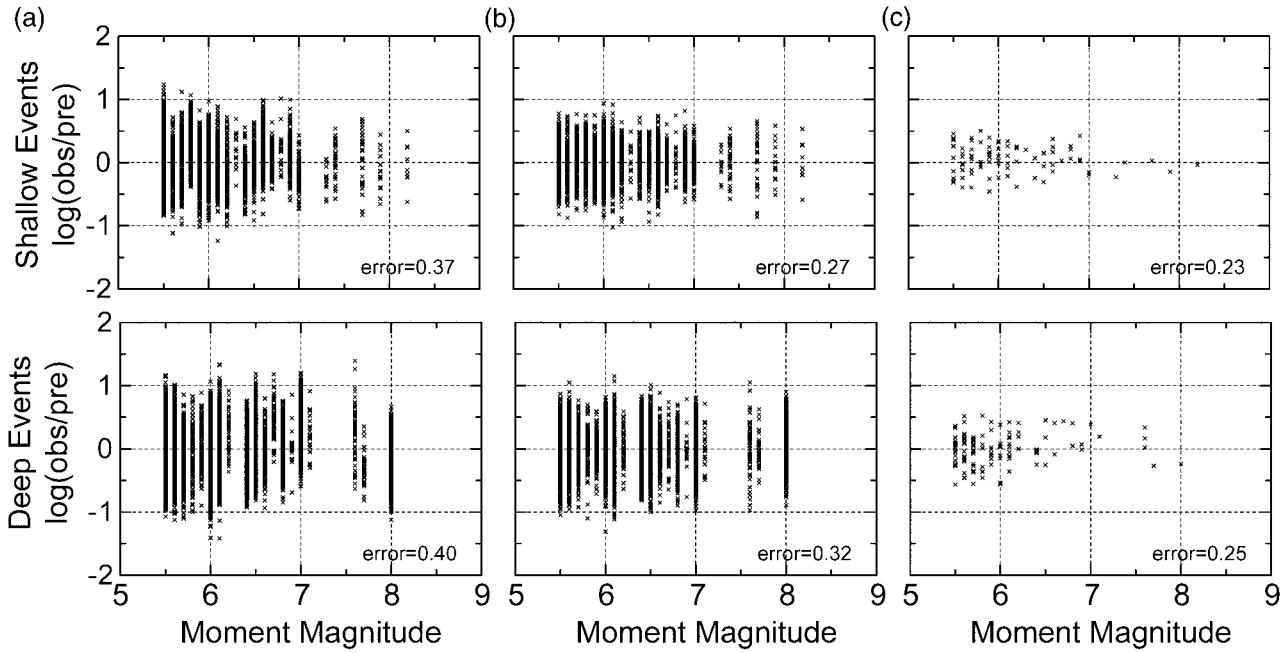

Figure 16. Relationship between residuals of PGA and moment magnitude: (a) total error; (b) intraevent error; (c) interevent error.

events in Japan and 788 records from 12 events in countries other than Japan. We selected 11,542 records from 184 events in Japan and 377 records from 10 events elsewhere for regression analysis.

- Two simple regression models were adopted for shallow (focal depth of 30 km or less) and deep (focal depth of more than 30 km) events.
- Additional correction terms accounting for site effects were introduced as a function of average shear-wave velocity from the ground surface to 30 m in depth (AVS30).
- The new standard attenuation relations used in this study are able to capture the strong-motion attenuation characteristics of sites with an AVS30 of approximately 300 m/sec.
- An additional correction term corresponding to the anomalous seismic intensity in northeast Japan improves the prediction accuracy for PGA and 5% damped acceleration response spectra at short periods.
- Residuals decrease with increasing predicted amplitude and decreasing source distance. Residuals seem to increase with focal depth for earthquakes shallower than 70 km. However, no focal-depth dependency of the residuals is clear for events deeper than 70 km.
- Distributions of total, intraevent and interevent errors with respect to moment magnitude are not biased.

Acknowledgments

We express our thanks to Dr. T. Ishii, Dr. T. Sato, Mr. T. Okumura, Dr. Y. Ishikawa, Dr. P. Somerville, Dr. J. Zhao, Dr. D. Spurr, Dr. A. Pitarka, an anonymous reviewer, and the committee on probabilistic seismic hazard map (Chairman: Prof. S. Midorikawa) who gave much valuable advice. We would like to acknowledge the following organizations and others, who kindly provided us with the strong-motion data: California Division of Water Resources, California Strong-Motion Instrumentation Program, Central Research Institute of Electric Power Industry, Earthquake Research Department, Hanshin Expressway Public Corporation, Honshu-Shikoku Bridge Authority, Japan Meteorological Agency, Japan Railway Company Group, Kandilli Observatory and Earthquake Research Institute, Kansai Electric Power Company, Kobe City Office, Konoike Construction Co., Ltd, Kyoto University, Los Angeles Department of Water and Power, Maeda Corporation, Matsumura-gumi Corporation, National Institute for Land and Infrastructure Management, National Research Institute for Earthquake Science and Disaster Prevention: K-NET and KiK-net, Nippon Telegraph and Telephone Corporation, Obayashi Corporation, Osaka Gas Co., Ltd., Port and Airport Research Institute, Railway Technical Research Institute, Shiga Prefecture, Southern California Edison, The Association for Earthquake Disaster Prevention, The Committee of Earthquake Observation and Research in the Kansai Area, The University of Shiga Prefecture, Tokyo Electric Power Company, United States Geological Survey, and the University of Southern California (in alphabetical order).

References

Annaka, T., F. Yamazaki, and F. Katahira (1997). A proposal of an attenuation model for peak ground motions and 5% damped acceleration response spectra based on the JMA-87 type strong motion accelerograms, in *Proc. 24th JSCE Earthquake Eng. Symposium*, 161–164 (in Japanese).

Aoi, S., K. Obara, S. Hori, K. Kasahara, and Y. Okada (2000). New strong-motion observation network: KiK-net, *EOS Trans. Am. Geophys. Union* **81,** 329.

Boore, D. M. (2001). Comparisons of ground motions from the 1999 Chi-Chi earthquake with empirical predictions largely based on data from California, *Bull. Seism. Soc. Am.* **91,** 1212–1217.

Boore, D. M., W. B. Joyner, and T. E. Fumal (1997). Equations for estimating horizontal response spectra and peak acceleration from Western North American earthquakes: a summary of recent work, *Seism. Res. Lett.* **68,** 128–153.

Building Seismic Safety Council (BSSC) (2000). The 2000 NEHRP recommended provisions for new buildings and other structures, Part I (Provisions) and Part II (Commentary), FEMA 368/369, Washington, D.C.

Campbell, K. W. (1981). Near-source attenuation of peak horizontal acceleration. *Bull. Seism. Soc. Am.* **71,** 2039–2070.

Chang, T.-Y., F. Cotton, and J. Angelier (2001). Seismic attenuation and peak ground acceleration in Taiwan, *Bull. Seism. Soc. Am.* **91,** 1229–1246.

Centroid Moment Tensor (CMT) catalog, Harvard University, www.seismology.harvard.edu/ (last accessed July 2005).

Consortium of Organizations for Strong-Motion Observation Systems (COSMOS), www.cosmos-eq.org (last accessed July 2005).

Fukushima, Y. (1996). Scaling relations for strong ground motion prediction models with M^2 terms, *Bull. Seism. Soc. Am.* **86,** 329–336.

Fukushima, Y. (1997). Comment on "Ground motion attenuation relations for subduction zones," *Seism. Res. Lett.* **68,** 947–949.

Fukushima, Y., and T. Tanaka (1990). A new attenuation relation for peak horizontal acceleration of strong ground motion in Japan, *Bull. Seism. Soc. Am.* **80,** 757–783.

Fukushima, Y., and T. Tanaka (1992). Revised attenuation relation of peak horizontal acceleration by using a new data base, *Progr. Abs. the Seism. Soc. Japan* **2,** 116 (in Japanese).

Fukushima, Y., C. Berge-Thierry, P. Volant, D. A. Griot-Pommera, and F. Cotton (2003). Attenuation relation for West Eurasia determined with recent near-fault records from California, Japan and Turkey, *J. Earthquake Eng.* **7,** no. 3, 1–26.

Fukushima, Y., K. Irikura, T. Uetake, and H. Matsumoto (2000). Characteristics of observed peak amplitude for strong ground motion from the 1995 Hyogo-ken Nanbu (Kobe) earthquake, *Bull. Seism. Soc. Am.* **90,** 545–565.

Fukuyama, E., M. Ishida, S. Hori, S. Sekiguchi, and S. Watada (1996). Broadband seismic observation conducted under the FREESIA Project, *Rep. Natl. Res. Inst. Earth Sci. Prev.* **57,** 23–31 (in Japanese with English abstract).

Headquarters for Earthquake Research Promotion (1995). www.jishin.go.jp/main/index-e.html (last accessed July 2005).

Idriss, I. M., and N. A. Abrahamson (2000). Geotechnical aspects of the earthquake ground motions recorded during the 1999 Chi-Chi earthquake, in *Proc. International Workshop Annual Commemoration Chi-Chi Earthquake*. Vol. 3, 9–22.

Kinoshita, S. (1998). Kyoshin net (K-net), *Seism. Res. Lett.* **69,** 309–334.

Kobayashi, H., and S. Midorikawa (1982). A semi-empirical method for estimating response spectra of near-field ground motions with regard to fault rupture, in *Proc. 7th European Conf. Earthquake Eng.* 161–168.

Lussou, P., P. Y. Bard, F. Cotton, and Y. Fukushima (2001). Seismic design regulation codes: contribution of K-net data to site effect evaluation, *J. Earthquak Eng.* **5,** 13–33.

Maeda, T., and T. Sasatani (2002). Upper mantle Qs structure beneath an island arc and strong ground motions from intra-slab earthquakes, in *Proc. 11th Japan Earthquak Eng. Symposium,* 505–510 (in Japanese with English abstract).

Matsuoka, M., and S. Midorikawa (1993). Empirical estimation of average shear-wave velocity of ground using the Digital National Land Information, *J. Struct. Constr. Eng. AIJ*, **443,** 65–71 (in Japanese with English abstract).

Midorikawa, S., and Y. Ohtake (2002). Attenuation relationships of peak ground acceleration and velocity considering attenuation characteristics for shallow and deep earthquakes, in *Proc. 11th Japan Earthquake Eng. Symposium*, 609–614 (in Japanese with English abstract).

Midorikawa, S., and Y. Ohtake (2003). Empirical analysis of variance of ground motion intensity in attenuation relationships, *J. Japan Assoc. Earthquake Eng.* **3-1,** 59–70 (in Japanese with English abstract).

Midorikawa, S., M. Matsuoka, and K. Sakugawa (1994). Site effects on strong-motion records observed during the 1987 Chiba-ken-toho-oki, Japan earthquake, in *Proc. 9th Japan Earthquak Eng. Symposium,* E-085-E-090.

Morikawa, N., and T. Sasatani (2004). Source models of two large intraslab earthquakes from broadband strong ground motions, *Bull. Seism. Soc. Am.* **94,** 803–817.

Morikawa, N., T. Kanno, A. Narita, H. Fujiwara, and Y. Fukushima (2003). Additional correction terms for attenuation relations corresponding to the anomalous seismic intensity in Northeast Japan, *J. Japan Assoc. Earthquake Eng.*, **3-4,** 14–26 (in Japanese with English abstract).

Nishimura, T., and M. Horike (2003). The attenuation relationships of peak ground acceleration for the horizontal and the vertical components inferred from the Kyoshin Network data, *J. Struct. Constr. Eng. AIJ* **571,** 63–70 (in Japanese with English abstract).

Sadigh, K., C.-Y. Chang, J. A. Egan, F. Makdisi, and R. R. Youngs (1997). Attenuation relationship for shallow crustal earthquakes based on California strong motion data. *Seism. Res. Lett.* **68,** 180–189.

Sato, R. (1989). *Fault Parameter Handbook in Japan*, Kajima Institute Publishing Co., Ltd., Tokyo (in Japanese).

Seno, T., K. Otsuki, and C.-N. Yang (2000). The 1999 Chi-Chi, Taiwan Earthquake: a subduction zone earthquake on land, *Bull. Earthquake Res. Inst.* **75,** 57–77.

Si, H., and S. Midorikawa (1999). New attenuation relationships for peak ground acceleration and velocity considering effects of fault type and site condition, *J. Struct. Constr. Eng. AIJ* **523,** 63–70 (in Japanese with English abstract).

Spudich, P., J. B. Fletcher, M. Hellweg, J. Boatwright, C. Sullivan, W. B. Joyner, T. C. Hanks, D. M. Boore, A. McGarr, L. M. Baker, and A. G. Lindh (1997). SEA96-A new predictive relation for earthquake ground motion in extensional tectonic regimes, *Seism. Res. Lett.* **68,** 190–198.

Takahashi, T., A. Asano, H. Okada, T. Saiki, K. Irukura, J. X. Zhao, J. Zang, H-K. Thio, P.G. Somerville, Y. Fukushima, and Y. Fukushima (2004). Attenuation relations of strong motion in Japan using site classification based on predominant period, Workshop on seismic input motions, incorporating recent geological studies, Committee on the Safety of Nuclear Installations (CSNI), OECD/NEA.

Umino, N., and A. Hasegawa (1984). Three-dimensional Qs structure in the northeastern Japan arc, *Zisin* **37,** 213–228 (in Japanese with English abstract).

Utsu, T. (1967). Anomalies in seismic wave velocity and attenuation associated with a deep earthquake zone, *J. Fac. Sci. Hokkaido Univ. Ser. VII (Geophys.)* **3,** 1–25.

Youngs, R. R., S. J. Chiou, W. J. Silva, and J. R. Humphrey (1997). Strong ground motion attenuation relationships for subduction zone earthquakes, *Seism. Res. Lett.* **68,** 58–73.

Zhao, J. X., K. Irikura, J. Zhang, Y. Fukushima, P. G. Somerville, A. Asano, T. Saiki, H. Okada, and T. Takahashi (2004). Site classification for strong-motion stations in Japan using H/V response spectral ratio, in *Proc. 13th World Conf. Earthquake Eng.*, paper no. 1278.

Tatsuo Kanno
Graduate School of Engineering
Hiroshima University
1-4-1, Kagamiyama, Higasni-Hiroshima
Hiroshima, 739-8527, Japan
tkanno@hiroshima-u.ac.jp
(T.K.)

Mitsubishi Space Software Co., Ltd.
Tsukuba Mitsui Building
1-6-1, Takezono, Tsukuba
Ibaraki, 305-0032, Japan
anarita@mi.mss.co.jp
(A.N.)

National Research Institute for Earth Science and Disaster Prevention
3-1, Tennodai, Tsukuba
Ibaraki, 305-0006, Japan
morikawa@bosai.go.jp
fujiwara@bosai.go.jp
(N.M., H.F.)

Institute of Technology
Shimizu Corporation
3-4-14, Etchujima, Koto-ku
Tokyo, 135-8530, Japan
yoshimitsu.fukushima@shimz.co.jp
(Y.F.)

Manuscript received 11 July 2005.